Acta Pharmaceutica Sinica B 2026;16(2):1140−1154

Chinese Pharmaceutical Association
Institute of Materia Medica, Chinese Academy of Medical Sciences

Acta Pharmaceutica Sinica B

www.elsevier.com/locate/apsb
www.sciencedirect.com

ORIGINAL ARTICLE

Skin-penetrating peptides derived from computational simulation improve transdermal absorption and facilitate topical treatment of melanoma

Sanjiang Du[a], Hanlin Wang[a,b], Feiyang Geng[a], Zongxu Zhang[a], Chenghao Liu[a], Weiyue Lu[a,c], Gang Wei[a,c,d,e,*]

[a]*Department of Pharmaceutics, School of Pharmacy, Fudan University & Key Laboratory of Smart Drug Delivery (Fudan University), Ministry of Education & National Key Laboratory of Advanced Drug Formulations for Overcoming Delivery Barriers, Shanghai 201203, China*
[b]*State Key Laboratory of Chemical Biology, Shanghai Institute of Materia Medica, Chinese Academy of Sciences, Shanghai 201203, China*
[c]*The Institutes of Integrative Medicine of Fudan University, Shanghai 200040, China*
[d]*Shanghai Engineering Research Center of ImmunoTherapeutics, Shanghai 201203, China*
[e]*Quzhou Fudan Institute, Quzhou 324003, China*

Received 22 January 2025; received in revised form 2 April 2025; accepted 3 April 2025

KEY WORDS

Cell-penetrating peptides;
Cutaneous administration;
Computational simulation;
Melanoma;
Floxuridine;
AlphaFold;
Transdermal drug delivery;
Penetratin

Abstract Transdermal drug delivery relies heavily on the skin permeability of therapeutic agents. In order to develop a peptide-based delivery strategy for promoting transdermal absorption, the key physicochemical factors influencing skin permeability are first identified through cell-penetrating peptides (CPPs) screening and computational simulation. Penetratin exhibits the most outstanding permeability and safety among CPPs from various origins, and positive surface patch area emerges as the key property correlated with skin permeability of the peptides. Based on these findings, a precise model to predict skin permeability of the peptides is established, leading to the computational redesign of penetratin's amino acid sequence. The transdermal delivery efficiency of optimized penetratin derivative (589WP) is significantly improved *in vitro* compared with wild-type penetratin and visualized through *in vivo* imaging. Furthermore, the anti-metabolic drug floxuridine (FUdR) is covalently conjugated with 589WP *via* ester linkage, leading to accelerated FUdR release due to esterase degradation. Subsequently, this conjugate is formulated into an anhydrous gel, which significantly inhibits melanoma growth with topical application,

*Corresponding author.
E-mail address: weigang@shmu.edu.cn (Gang Wei).

Peer review under the responsibility of Chinese Pharmaceutical Association and Institute of Materia Medica, Chinese Academy of Medical Sciences.

https://doi.org/10.1016/j.apsb.2025.12.026

outperforming a higher dose of free FUdR without observed skin irritancy or toxicity. The peptide prediction and design approaches established herein hold great potential for advancing transdermal drug delivery.

1. Introduction

Transdermal drug delivery systems (TDDS) offer numerous advantages, including consistent and stable plasma levels, avoidance of the first-pass effect in the liver, good patient compliance, and cessation of treatment as needed, all of which are highly significant in medical practice[1−3]. However, the skin, being the body's natural protective barrier, exhibits low permeability to most small molecules, which restricts the entry of pathogens and toxins but also hinders transdermal drug delivery[4,5]. The primary permeation barrier in the skin is the outermost layer, the stratum corneum, consisting of tightly packed and highly keratinized dead cells embedded in a lipid matrix[6,7]. Therefore, for transdermal delivery, the drugs must penetrate through the intricate lipid pathways surrounding the keratin-rich cells, or repeatedly partition between these cells and the lipid matrix, or traverse the skin appendage pathways. In general, strategies that promote transdermal drug delivery can be categorized into two classes: active or passive means. Active means include iontophoresis, sonophoresis, electroporation, microneedles, and so on, while passive means include permeation enhancers and various nanoscale delivery systems[8−10].

As novel skin permeation enhancers, peptides have garnered much attention in the last two decades. Peptide-based drug delivery systems offer advantages such as excellent biodegradability and biocompatibility[11,12], avoiding safety concerns associated with traditional chemical enhancers and substantially improving the feasibility of clinical translation. There are three categories of peptides with efficient skin permeability, including cell-penetrating peptides (CPPs), antimicrobial peptides (AMPs), and phage peptides[13]. CPPs are typically made up of 5−30 amino acids and can be utilized as molecular transporters to facilitate the passage of therapeutic agents across physiological barriers[14,15]. AMPs are known to form pores in bacterial cell membranes, and have been shown to increase skin permeability by disrupting the stratum corneum lipid structure[16,17]. Phage peptides are obtained by phage display technology, where a random amino acid sequence is displayed on each phage particle, and libraries of such peptides can be screened for skin penetration[18,19].

In the field of TDDS, the mechanisms governing the skin penetration of peptides have not been fully elucidated due to variations in the physicochemical properties of different peptides. These specific mechanisms include interactions between peptides and keratin[20,21], increased lipid fluidity[22,23], peptide transduction domains[24,25], shielding of drug negative charges[26,27], amphipathy[28], reversible modulation of intercellular junction proteins[29], etc. In these studies, peptides are employed as permeation enhancers, primarily through covalent conjugation with drugs[30,31], while in some cases, they are applied non-covalently with the drugs[32,33]. These approaches have increased the skin permeability of various agents by several to dozens-fold. However, due to the lack of systematic comparison, optimization, and theoretical guidance, the design of peptides as efficient transdermal enhancers was deficient in reliable predictive models and primarily explored by the trial-and-error process. Thus, there remains still ample room for improving transdermal drug delivery efficiency.

AlphaFold2, developed by DeepMind, is a revolutionary tool for predicting the three-dimensional structures of proteins and peptides. Traditional experimental methods like X-ray crystallography and nuclear magnetic resonance (NMR) spectroscopy, though accurate, are both time-consuming and costly. Moreover, they also struggle with certain proteins or peptides that are difficult to crystallize or are highly dynamic. This emphasizes the need for efficient computational approaches to complement experimental techniques[34]. Utilizing deep learning, AlphaFold2 compares protein sequences with extensive databases of known structures, leveraging evolutionary information and physicochemical principles to achieve near-experimental accuracy in its predictions[35].

Melanoma is the most aggressive and fatal form of skin cancer[36]. Systemic chemotherapies against melanoma exhibit limited antitumor potential and high toxicity[37]. TDDS can deliver therapeutic molecules directly to the site of melanoma, making it a promising treatment approach. Floxuridine (5-fluoro-2′-deoxyuridine, FUdR) is a metabolite of 5-fluorouracil (5-FU) and can be convert to 5-FU by thymidine phosphorylase[38]. It exerts antitumor effects through the inhibition of thymidylate synthase and incorporation of its metabolites into RNA and DNA[39]. 5-FU cream is recommended for topical therapy of basal cell carcinomas[40], a type of skin cancer, and it has been approved by the US Food and Drug Administration (FDA) for clinical application[41,42]. However, due to the limited skin permeability of hydrophilic 5-FU and FUdR, their topical administration typically requires high concentrations, usually 2.5% or 5%, increasing the risk of side effects such as skin erythema, itching, and burning sensation[43].

In this research, we systematically compared, analyzed, and predicted the skin permeabilities of CPPs from different sources with the assistance of computational simulation. We tried to elucidate the key factors determining transdermal delivery efficiency, considering aspects of peptide structure depicted by AlphaFold2 algorithm and corresponding physicochemical properties. Our investigation aimed to reveal the underlying principles and develop novel approaches for designing skin-penetrating peptides. Building on these findings, we identified the optimized peptide derivatives and validated their application in the topical delivery of FUdR for treatment of melanoma.

2. Materials and methods

2.1. Materials

Peptides and fluorescence-labeled peptides were synthesized by Allpeptide Biotechnology, Hangzhou, China. Floxuridine

(5-fluoro-2'-deoxyuridine, FUdR), dimethyl sulfoxide (DMSO), acetonitrile, 4-maleimidobutyric acid, 4-dimethylaminopyridine (DMAP), *N*,*N*'-dicyclohexylcarbodiimide (DCC) were purchased from Aladdin Industrial Corporation, Shanghai, China. Phosphate buffer solution (PBS), 5-carboxyfluorescein (FAM), Cy5 *N*-hydroxy succinimide ester (Cy5-NHS), glycerin, polyethylene glycol (PEG) 200, PEG 400, Cell Counting Kit-8 (CCK-8), Calcein-AM/PI double staining kits were commercially obtained from MeilunBio, Dalian, China. All other reagents used in the experiment were of analytical grade and no further purification was required. Hematoxylin-eosin (HE) staining solution and IL-1β antibody were provided by Servicebio Technology, Wuhan, China.

2.2. Animals

Sprague−Dawley (SD) rats, Institute of Cancer Research (ICR) mice, and C57BL/6 mice were provided by Laboratory Animal Center of School of Pharmacy, Fudan University (Shanghai, China). The skin of Berkshire pig was provided by Meisheng Trading Company (Chongqing, China). All the animal experiments were performed following the guidelines evaluated and approved by the Institutional Animal Care and Use Committee (IACUC), School of Pharmacy, Fudan University (Ethical approval number: 2020-04-YJ-WG-01).

2.3. In vitro skin penetration

The purity and molecular weight of FAM-labeled peptides were verified using High Performance Liquid Chromatography (HPLC, Agilent, 1260, SC, USA) and mass spectrometry (MS, AB Sciex, 4000 Q TRAP, MA, USA), respectively. The skin permeability of FAM and FAM-CPPs was investigated for rats and pigs. All the CPPs were conjugated with FAM at the N-terminus, and their concentrations were measured based on fluorescence intensity. In brief, 1 mmol of FAM or FAM-peptide was initially dissolved in 100 μL DMSO and then further diluted with 20 mL of 0.9% NaCl solution, resulting in a final solution containing 50 μmol/L FAM or FAM-peptide and 0.5% (*v*/*v*) DMSO. The transdermal penetration experiment was carried out using the Valia-Chien diffusion cells (Kaiyue, TK-6H1, Shanghai, China). The experiment temperature was maintained by a water bath at 37 ± 0.5 °C with a stirring speed of 250 rpm. Each diffusion cell had a volume of 3.5 mL, and the skin samples were obtained from either SD rats or Berkshire pigs. All the *in vitro* skin penetration experiments were performed in at least 4 replicates for each peptide to enhance the statistical significance and reliability of the results.

At time points 0, 0.5, 1, 2, 3, 4, and 5 h, 0.2 mL of receiver solution was withdrawn and immediately replaced with an equal volume of fresh 0.9% NaCl solution. Fluorescence intensity was immediately measured at 492 nm using the multimode reader (BioTek, Synergy 2, VT, USA). The calculation formula for the *in vitro* data is as Eq. (1):

$$Q_t = V_r \times C_t + \int_{t=0}^{t-1} V_s \times C_i \quad (1)$$

where Q_t is the cumulative penetration amount of the drug, C_t is the drug concentration of the receiver solution at each sampling time, C_i is the drug concentration of the sample, and V_r and V_s are the volumes of the receiver solution and the sample, respectively. The obtained data were expressed as the cumulative drug permeation per unit of skin surface area, Q_t/S. Apparent permeability coefficient (P_{app}) was calculated by linear regression interpolation of the experimental data, as shown by Eq. (2):

$$P_{app} = \frac{\Delta Q}{\Delta t \times S \times C_0} \quad (2)$$

where C_0 is the drug concentration in the donor compartment (50 μmol/L), while the drug content in the receiver is negligible compared with that in the donor.

2.4. Physicochemical parameters of peptides

The folding structures of peptides were predicted using the AlphaFold2 algorithm (DeepMind Technologies, AlphaFold2, London, UK) based on ColabFold (Google Research, ColabFold v1.5.2, CA, USA). The predictions were made following the instructions available at https://colab.research.google.com/github/sokrypton/ColabFold/blob/main/AlphaFold2.ipynb#Instructions[44]. ColabFold was combined with MMseqs2's fast homology search and AlphaFold2 or RoseTTAFold to accelerate the prediction of protein structures. ColabFold predicts protein structures through AlphaFold2 and Alphafold-Multimer, where sequence alignments/templates were generated through MMseqs2 and HHsearch.

Then various physicochemical parameters of peptides were computed using the Maestro software (Schrödinger, Maestro 2020-2, NY, USA)[45]. Surface areas for all peptides were computed and visualized using the Protein Surface Analyzer module. The OPLS3e force field was utilized for the calculation protocol. All initial structures were prepared and processed through the Protein Preparation Wizard function. Notably, energy minimization was intentionally omitted, as the AlphaFold2 algorithm had already determined the 3D fold structure, and applying energy minimization could alter the structure.

The MilogP value was calculated using the website www.molinspiration.com.

2.5. Prediction of peptide sequences

The prediction was conducted by introducing mutations into the amino acid sequence of wild-type penetratin. The maximum allowable mutations were limited to 3. The positive surface patch area (PSPA) and hydrophobic surface patch area (HSPA) values for these mutated sequences were computed. The top 3 peptide sequences with the highest PSPA or score of amphipathy (SOA) values were the focus of our investigation. These selected sequences were then subjected to *in vitro* skin penetration testing.

2.6. Preparation of Cy5-589WP gel

The anhydrous gel matrix consisted of 50% (*w*/*w*) glycerin, 30% PEG 200, and 20% PEG 400. To synthesize the Cy5-589WP conjugate, 3.0 mg Cy5-NHS and 4.9 mg 589WP were weighed and dissolved in 1 mL PBS buffer (pH 8.3) and stirred at 4 °C for 3 h. The conjugate was purified by preparative HPLC (Agilent, Prep-1260, SC, USA) and lyophilization (Zirbus, VaCo5, Bad Grund, Germany). Subsequently, 1.58 mg of the lyophilized powder was reconstituted in 3 mL of the gel matrix to achieve a final concentration of 0.525 mg/mL Cy5-589WP solution (equivalent to Cy5 0.2 mg/mL). Similarly, 0.6 mg Cy5 was dissolved with 3 mL of the gel matrix to yield a 0.2 mg/mL Cy5 solution.

2.7. *In vivo skin penetration*

To further investigate the skin permeability of 589WP *in vivo*, merged images of fluorescence molecular tomography (FMT) and computed tomography (CT) were captured using the *vivo* imaging system (Caliper PerkinElmer, IVIS Spectrum, MA, USA). The dorsal hair of ICR mice was shaved to the minimum length, and 20 μL of Cy5 or Cy5-589WP gel was administered along the centerline of the back. At the 0 h time point, photographs of the mice were recorded with the gels on their back. After 4 or 8 h of administration, the gels were carefully wiped using wet cotton balls. Subsequently, photographs of the mice were recorded to observe the fluorescent probes that penetrated the skin.

2.8. *Synthesis of FUdR-589WP*

Initially, 250 mg of FUdR (1.0 mmoL) was dissolved in 25 mL of acetonitrile. Simultaneously, 186.8 mg of 4-maleimidobutyric acid (1.0 mmoL) as the linker, 12.4 mg of DMAP (0.1 mmoL), and 230.7 mg of DCC (1.1 mmoL) were dissolved separately in 3 mL of dichloromethane. The FUdR and DCC solutions were mixed and allowed to react at room temperature for 2 h. Subsequently, the solutions of DMAP and the linker were added to the reaction mixture, which was then stirred at room temperature overnight. The mixture was then filtered, and the filtrate was collected. The solvent was removed by rotary evaporation (Shen Sheng Technology, R213, Shanghai, China), and the residue was resuspended in 7.2 mL of ultrapure water-methanol (1:1, *v*/*v*) using sonication. Purification was performed using preparative HPLC, followed by lyophilization. The product FUdR-MAL was verified using ^{1}H NMR (Varian, 400 MHz, CA, USA) and MS.

10 mg of FUdR-MAL and 62.1 mg of Cys-589WP were dissolved individually in 10 mL of methanol. After mixing, 10 μL of triethylamine was added, and the mixture was allowed to react at 37 °C on a shaker for 30 min. Methanol and triethylamine were subsequently removed by rotary evaporation, and the residue was then resuspended in an appropriate solvent using sonication. The crude product was purified by preparative HPLC, followed by lyophilization. The final product FUdR-589WP was verified using MS.

2.9. *In vitro cytotoxicity*

The cytotoxicity of various CPPs, 589WP, FUdR, FUdR-Mal, and FUdR-589WP against B16F10 cells was assessed using the CCK-8 assay kit. The cells were seeded in 96-well plates and after 24 h incubation, a series of solutions at various concentrations were co-incubated with the cells for 48 h. Subsequently, the cytotoxicity was detected by CCK-8 solution. The absorbance values of each well were measured at 450 nm with the multimode reader (BioTek). To visualize the difference in cytotoxicity, B16F10 cells were treated with 15 μmol/L agents for 48 h. Subsequently, the cells were stained using the Calcein-AM/PI double staining kits and observed under an inverted fluorescence microscope (Leica Microsystems, DMI4000D, Hesse, Germany).

2.10. *In vitro drug release*

The release of FUdR from the conjugate FUdR-589WP in solution was investigated. The FUdR-589WP solutions were prepared using PBS buffer (pH 5.5, 6.5, 7.4, or 8.3) to achieve a final concentration of 0.5 mmol/L FUdR-589WP and a pig liver esterase concentration of 0, 3, or 30 U/mL. Under a condition of 37 °C and 200 rpm, the concentrations of released FUdR were measured using HPLC at 1, 2, 4, 8, 24, 48, and 96 h.

2.11. *Preparation of FUdR-589WP gel*

The composition of the anhydrous gel matrix was identical to that of Cy5-589WP gel. The blank gel consisted solely of the gel matrix. The FUdR gel contained free FUdR at a concentration of either 0.5% or 2.5% (*w*/*w*). The FUdR/589WP gel was prepared through physical mixing of FUdR and 589WP at a 1:1 M ratio, resulting in a final FUdR concentration of 0.5% (*w*/*w*). The FUdR-589WP gel contained a covalent compound of FUdR and 589WP, with a final FUdR concentration of either 0.05% or 0.5% (*w*/*w*).

2.12. *Anti-tumor efficacy*

To evaluate whether FUdR-589WP gel could improve skin penetration and enhance *in viv*o therapeutic efficacy, a subcutaneous xenograft tumor model was established by inoculating B16F10 cells (1×10^6) in the left back of the male C57BL/6 mice. The mice were randomly divided into six groups: (i) blank gel, (ii) 0.5% FUdR gel, (iii) 2.5% FUdR gel, (iv) 0.5% FUdR/589WP gel, (v) 0.05% FUdR-589WP gel, and (vi) 0.5% FUdR-589WP gel. Treatment commenced when the tumor reached an approximate volume of 100 mm^3, with 30 μL gel administered to the skin once a day. The mice were euthanized when the tumors grew to a volume of approximately 2000 mm^3. Their main organs (liver, kidney, lung, spleen, heart) and the skin covering the melanoma were collected for histopathological analysis using HE staining.

2.13. *Skin irritancy*

Healthy C57BL/6 mice were used to evaluate skin irritation caused by the gels. The mice were randomly divided into five groups: (i) blank gel, (ii) 0.5% FUdR gel, (iii) 2.5% FUdR gel, (iv) 0.5% 589WP gel, and (v) 0.5% FUdR-589WP gel. Thirty microliters of gel were administered to the skin once daily, and the mice were euthanized after 7 days of administration. Skin samples from the administration site were collected for immunohistochemical staining with the IL-1β antibody to assess the degree of inflammation as an indicator of skin irritation.

2.14. *Statistical analysis*

All statistical data analyses were performed using GraphPad Prism 8 software. The two-tailed, unpaired Student's *t*-test was used for comparation between two groups. One-way analysis of ANOVA and Tukey's *post hoc* tests were used when more than two groups were compared. Data are expressed as mean ± standard deviation (SD). A significant level of $P < 0.05$ was considered statistically significant for all tests.

3. Results

3.1. *Screening for outstanding skin-penetrating peptide among CPPs*

The major challenge for drugs delivered transdermally is their limited ability to penetrate intact skin. Enhancing permeability holds the benefit of improving drug absorption and efficacy while

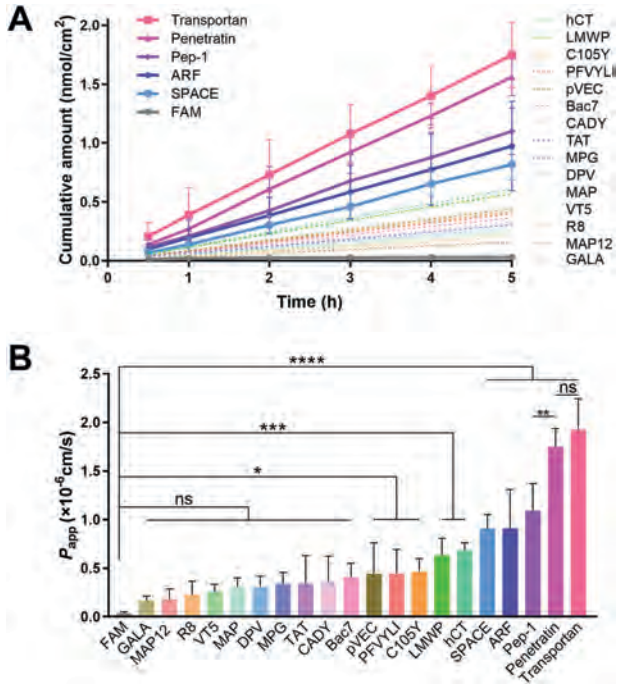

Figure 1 Skin permeability of FAM−CPP conjugates across excised rat skin. (A) Cumulative amount-time curves of FAM and FAM−CPP conjugates across excised rat back skin. (B) Corresponding apparent permeability coefficients (P_{app}) of FAM and FAM−CPP conjugates. All CPPs were conjugated with FAM at the N-terminus, and concentrations were measured based on fluorescence intensity. The donor chamber contained 50 μmol/L concentration of either FAM or FAM−CPP conjugates. Data are presented as mean ± SD (n = 4−5). *P < 0.05, **P < 0.01, ***P < 0.001, and ****P < 0.0001 *vs*. indicated; ns, not significant.

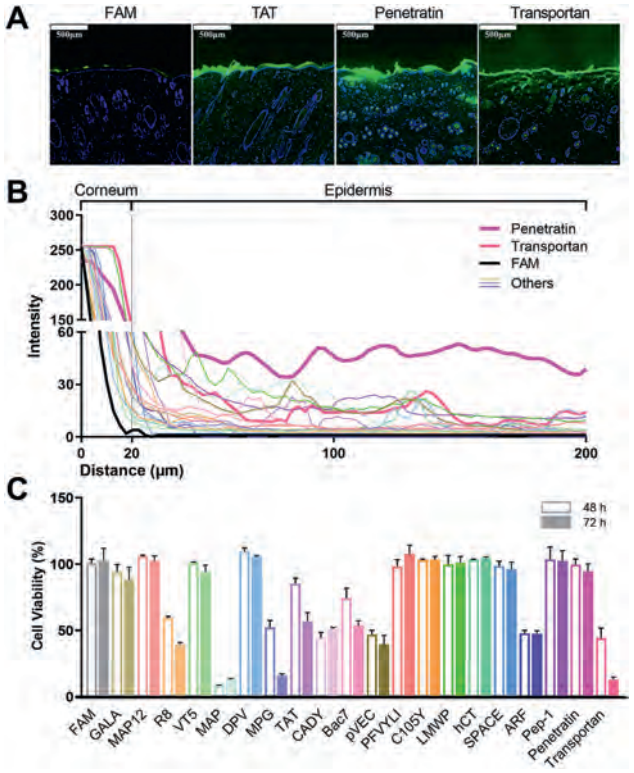

Figure 2 *Ex vivo* distribution in rat skin and cellular toxicity of FAM−CPP conjugates. (A) Merged fluorescence images of free FAM and FAM-labeled TAT, penetratin, and transportan. (B) Distribution of fluorescence within 200 μm depth of excised rat skin. (C) Heka cell viability after administration of 50 μmol/L FAM or FAM−CPP conjugates for 48 and 72 h (n = 3). Frozen sections of skin exposed to either FAM or FAM−CPP conjugates were visualized in merged images displaying DAPI and FAM fluorescence (Scale bar = 500 μm). The penetration depth of FAM−CPP conjugates along the arrow was depicted in the intensity-distance curves. For the convenience of comparison, the maximum fluorescence intensity of all groups was normalized to 255. Cell viability was determined using the Cell Counting Kit-8 (CCK-8).

reducing potential side effects. Therefore, we selected 20 kinds of known CPPs from various sources and labeled them with fluoresceinamine (FAM) (Details in Supporting Information Table S1). Then, we performed a comparison between the skin permeability of free FAM and these FAM-CPP conjugates using excised rat skin. The results are depicted by the cumulative amount-time curves (Fig. 1A) and the apparent permeability coefficients (P_{app}) (Fig. 1B). All the cumulative amounts of the conjugates in the receiver chamber were linearly increased with time, revealing the transdermal permeation was mainly driven by passive diffusion. The P_{app} value of free FAM was only 3.42×10^{-8} cm/s, while the P_{app} value of the FAM-CPP conjugates ranged from 1.71×10^{-7} to 1.92×10^{-6} cm/s, which meant that the skin permeability of FAM had been improved by 5 to 56 times. Meanwhile, the improvement effects induced by the CPPs revealed great differences. For CPPs GALA, MAP12, R8, VT5, MAP, DPV, MPG, TAT, CADY, and Bac7, there was no significant difference in their P_{app} values compared to free FAM ($P > 0.05$). In contrast, for CPPs pVEC, PFYLI, C105Y, LMWP, hCT, SPACE, ARF, Pep-1, penetratin, and transportan, they demonstrated significantly higher permeability than free FAM ($P < 0.05$ to $P < 0.0001$). Notably, penetratin and transportan displayed outstanding skin permeability, which was significantly higher than the other CPPs ($P < 0.01$).

To visualize penetration depth and distribution of FAM-CPP conjugates, we examined frozen sections of the recovered skin from the *ex vivo* evaluation under a fluorescence microscope. The typical images are presented in Fig. 2A, and full sets are provided in Supporting Information Fig. S1. Clear differences in both penetration depth and fluorescence distribution distinguished penetratin and transportan from other CPPs. Furthermore, penetratin exhibited a continuously high-level distribution compared to other peptides within 200 μm of the outermost skin (Fig. 2B), which meant it penetrated the complete stratum corneum and epidermis efficiently. Importantly, compared to transportan, penetratin did not display cytotoxicity even after exposure to human keratinocyte cells (HeKa cells) for 72 h (Fig. 2C). In addition, penetratin is composed of only 16 amino acids, substantially shorter than transportan (27 amino acids). Considering both safety and cost-effectiveness, penetratin was selected for further modification.

3.2. Correlations between P_{app} values and physicochemical parameters of peptides

To identify the key parameters influencing skin permeability, we computed various physicochemical properties of the peptides

using the AlphaFold2 algorithm and Maestro software (Supporting Information Table S2). Subsequently, we analyzed these parameters correlated with P_{app} values. When all peptides were analyzed together, we found that no individual physicochemical parameter of the peptides exhibited a good correlation with the P_{app} values, as demonstrated by the correlation coefficient (r) value lower than 0.5 (Fig. 3A), and no general rule emerged. The poor correlations may be attributed to variations in the mechanisms of membrane permeability among different peptides. However, for specific classifications of peptides, such as cationic, amphipathic, and hydrophobic peptides, certain correlation coefficients exceeded 0.5, including molecular weight (MW), charge, number of basic residues (NBR), hydrogen bond donor area (HBDA), hydrophobic moment (HM), positive surface patch area (PSPA), sum of agg-score (SA), and hydrophobic surface patch area (HSPA) (Fig. 3B−D). This improvement likely reflects shared structural features within each class. For instance, amphipathic peptides often exhibit similar secondary structures, including α-helix or β-sheet[46]. Furthermore, we observed the correlation coefficients between P_{app} values and parameters PSPA, charge, and HBDA

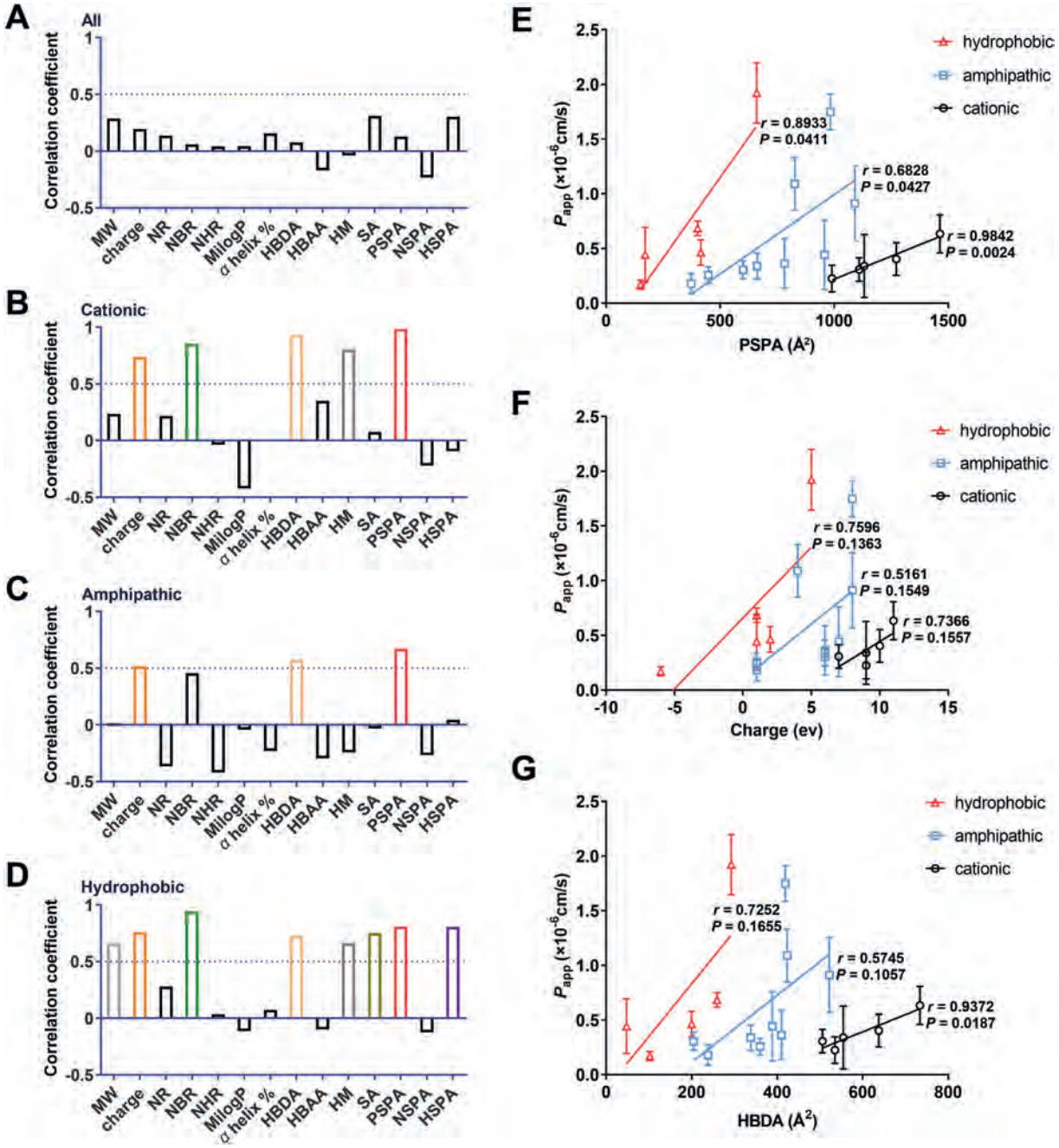

Figure 3 Revealing key parameters in skin permeability through statistical analysis. (A−D) Correlation coefficients between P_{app} values and various physicochemical parameters for different classifications of peptides: (A) all CPPs, (B) cationic CPPs, (C) amphipathic CPPs, (D) hydrophobic CPPs. (E−G) Correlations between P_{app} value and (E) PSPA, (F) charge, (G) HBDA. All correlation analyses were based on Pearson correlation coefficients, with P-values calculated using a two-tailed test. Data are presented as mean ± SD (n = 4−5).

exceeded 0.5 for all cationic, amphipathic, and hydrophobic peptides (Fig. 3E−G). However, only the correlations of PSPA were statistically significant ($P = 0.0411$ for hydrophobic peptides, $P = 0.0427$ for amphipathic peptides, and $P = 0.0024$ for cationic peptides). Thus, PSPA is the primarily predictor of peptide skin permeability.

3.3. Refinement of prediction model and optimization of peptide sequences

We developed two prediction models based on single-factor or two-factor fitting, respectively. In the single-factor fitting model, the skin permeability was supposed to increase with PSPA. Single

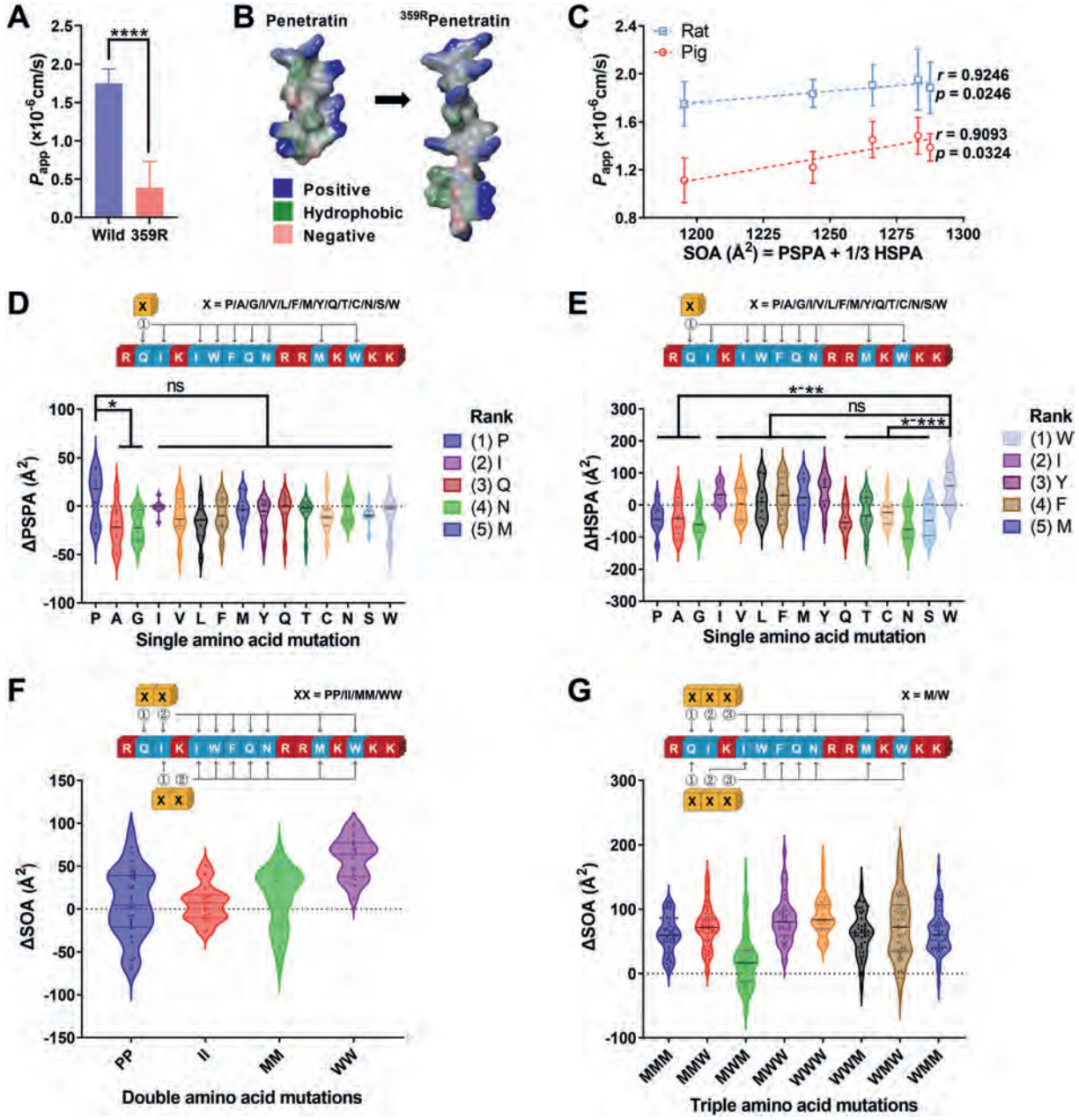

Figure 4 Optimizing the fitting model based on amphipathy and predicting peptide sequences. (A) Experimentally measured P_{app} values for wild-type penetratin and its derivative ^{359R}Penetratin, predicted by single-factor fitting. (B) Calculated surface patch area distribution for wild-type penetratin and ^{359R}Penetratin (Blue represents the positive surface patch, green represents the hydrophobic surface patch, and pink represents the negative surface patch). (C) Correlations between P_{app} values and SOA (score of amphipathy) in rat and pig skin. (D) Impact of single amino acid mutation on PSPA. (E) Impact of single amino acid mutation on HSPA. (F) Impact of two amino acid mutations on SOA. (G) Impact of three amino acid mutations on SOA. Four penetratin derivatives were synthesized to refine our fitting model. Calculations of PSPA, HSPA, and surface patch area distribution were performed using Maestro software (Schrödinger), and the top five amino acids improving PSPA or HSPA were listed on the right. Each point in Fig. 4D−G represents a peptide sequence, and the diagrams in the upper sections of Fig. 4D−G illustrate the logic behind the mutations. Data are presented as mean ± SD ($n = 4$). *$P < 0.05$, *-** $0.001 < P < 0.05$, *-*** $0.0001 < P < 0.05$, and ****$P < 0.0001$ *vs.* indicated; ns, not significant.

acidic amino acid mutation significantly reduced PSPA, while single basic amino acid mutation significantly increased PSPA (Supporting Information Fig. S2A), so we chose to introduce lysine and arginine for penetratin modification. When the substituted amino acids were restricted to less than three, the derivatives of three arginine (RRR) mutations (for example, ^{359R}Penetratin) exhibited the highest increases in PSPA (Fig. S2B). However, the determined P_{app} value of ^{359R}Penetratin was significantly reduced compared to the wild-type penetratin (Fig. 4A), which meant skin permeability of the predicted peptide did not align well with the single-factor fitting model. From the molecular conformation perspective, ^{359R}Penetratin showed a looser structure than the wild-type penetratin (Fig. 4B). This discrepancy suggests that PSPA is not the sole determinant of skin permeability.

To refine the prediction model, we synthesized four derivatives of wild-type penetratin, which were ^{28W}Penetratin, ^{29W}Penetratin, ^{89W}Penetratin, and ^{289W}Penetratin, respectively. Their sequences are listed in Table 1. We proposed a two-factor fitting model, which was defined as the score of amphipathy (SOA) and could be presented by the equation "SOA = PSPA + 1/3 HSPA", where the coefficient "1/3" was determined through the best linear fitting. When we conducted a fitting analysis based on SOA and the P_{app} data, the r values exceeded 0.9 for both rat and pig skin (Fig. 4C), leading to significant improvements in correlations ($P = 0.0246$ for rat skin and $P = 0.0324$ for pig skin). It's worth noting that PSPA and HSPA are interdependent variables, meaning that changes in PSPA inevitably lead to changes in HSPA. Therefore, the inclusion of HSPA in optimizing the model was reasonable and also based on an understanding of amphipathy.

Using the refined two-factor fitting model, we aimed to predict peptide sequences with the best skin permeability. To reduce computational complexity, we simplified the process into three steps—single, double, and triple mutations—instead of performing extensive calculations directly on triple mutations. Initially, we evaluated the impacts of single amino acid (excluding acidic and basic amino acids) mutation on both PSPA and HSPA (Fig. 4D and E). Notably, mutations with amino acids proline (P) and tryptophan (W) ranked first in terms of ΔPSPA and ΔHSPA, respectively, while isoleucine (I) and methionine (M) ranked in the top five for both ΔPSPA and ΔHSPA. Consequently, we selected P, W, I, and M to perform predictions of double amino acid mutations (Fig. 4F). Among the various mutated penetratin derivatives, two tryptophan (WW) and two methionine (MM) combinations demonstrated the top two rankings and exhibited better distributions of ΔSOA. Therefore, our final prediction of triple amino acid mutations was based on the combination of M and W (Fig. 4G). To prevent excessive disturbance of peptide structure, no more than three mutations were introduced.

3.4. Verification of transdermal penetration enhancement of optimized peptides

After comparing more than 1500 peptide sequences, three penetratin derivatives (^{589W}Penetratin, ^{3M89W}Penetratin, and ^{2W89M}Penetratin) were selected and synthesized based on the above calculations (Table 1). Their cumulative amount-time curves are depicted in Fig. 5A and B. As predicted, the P_{app} values of these peptides in both rat and pig skin showed a remarkable improvement (Fig. 5C). Among them, ^{589W}Penetratin (589WP) performed best. Moreover, these peptides conformed to the SOA fitting model in both rat ($r = 0.7824$, $P = 0.0218$) and pig ($r = 0.8689$, $P = 0.0051$) skin. Additionally, to reveal the effect of temperature on skin permeability, we compared the P_{app} values of fluorescence-labeled 589WP at 32 and 37 °C; however, the impact was minimal (Supporting Information Fig. S3).

To visualize the transdermal penetration efficacy of the peptide *in vivo*, fluorescence molecular tomography (FMT) and computed tomography (CT) images were recorded after the application of anhydrous gels loading with free Cy5 or Cy5-labeled 589WP (Fig. 5D). Initially, both Cy5 and Cy5-589WP gels displayed similar fluorescence intensity at the administration site. Four or 8 h later, the gels were wiped off using wet cotton balls before the mice were photographed. The mice treated with free Cy5 showed no discernible fluorescence at 4 h, while the mice in Cy5-589WP group exhibited significant fluorescence at the application site and even in their body. At 8 h, the fluorescence intensity of Cy5-589WP group was significantly stronger than that of Cy5 group. Meanwhile, The semi-quantitative results indicated a significant difference ($P < 0.0001$) in the residual amount of fluorescence between the Cy5 and Cy5-589WP groups at both 4 and 8 h (Fig. 5E). These results indicated that the peptide 589WP effectively facilitated transdermal absorption of fluorescent probe Cy5 through covalent conjugation.

Comparing wild-type penetratin with the derivatives ^{2W89M}Penetratin, ^{3M89W}Penetratin, and ^{589W}Penetratin, we observed that they maintained similar folding structures, and exhibited larger HSPA due to the introduction of extra hydrophobic tryptophan and methionine (Fig. 5F). From the perspective of the three-dimensional structure of peptides, it was the replacement of hydrophobic surface patches for some of the negative surface patches, as well as slight changes in the folded

Table 1 Sequences and characteristics of penetratin and its derivatives.

Name	Sequence	PSPA (Å)	HSPA (Å)	P_{app} in rat skin ($\times 10^{-6}$ cm/s)	P_{app} in pig skin ($\times 10^{-6}$ cm/s)
Penetratin	RQIKIWFQNRRMKWKK	983.2	636.3	1.75 ± 0.25	1.11 ± 0.26
^{28W}Penetratin	RWIKIWFWNRRMKWKK	967	829.6	1.83 ± 0.12	1.21 ± 0.14
^{29W}Penetratin	RWIKIWFQWRRMKWKK	975.5	871.1	1.90 ± 0.17	1.45 ± 0.17
^{89W}Penetratin	RQIKIWFWWRRMKWKK	996.7	858.9	1.95 ± 0.25	1.48 ± 0.17
^{289W}Penetratin	RWIKIWFWWRRMKWKK	976.1	934.3	1.88 ± 0.22	1.39 ± 0.18
^{589W}Penetratin	RQIKWWFWWRRMKWKK	1047.7	965.3	2.47 ± 0.21	1.80 ± 0.13
^{3M89W}Penetratin	RQMKIWFWWRRMKWKK	1088.7	884.9	2.10 ± 0.17	1.62 ± 0.15
^{2W89M}Penetratin	RWIKIWFMMRRMKWKK	1021.0	1004.2	1.97 ± 0.19	1.44 ± 0.16

Data are presented as mean ± SD ($n = 4$).
PSPA, positive surface patch area; HSPA, hydrophobic surface patch area; P_{app}, apparent permeability coefficients.

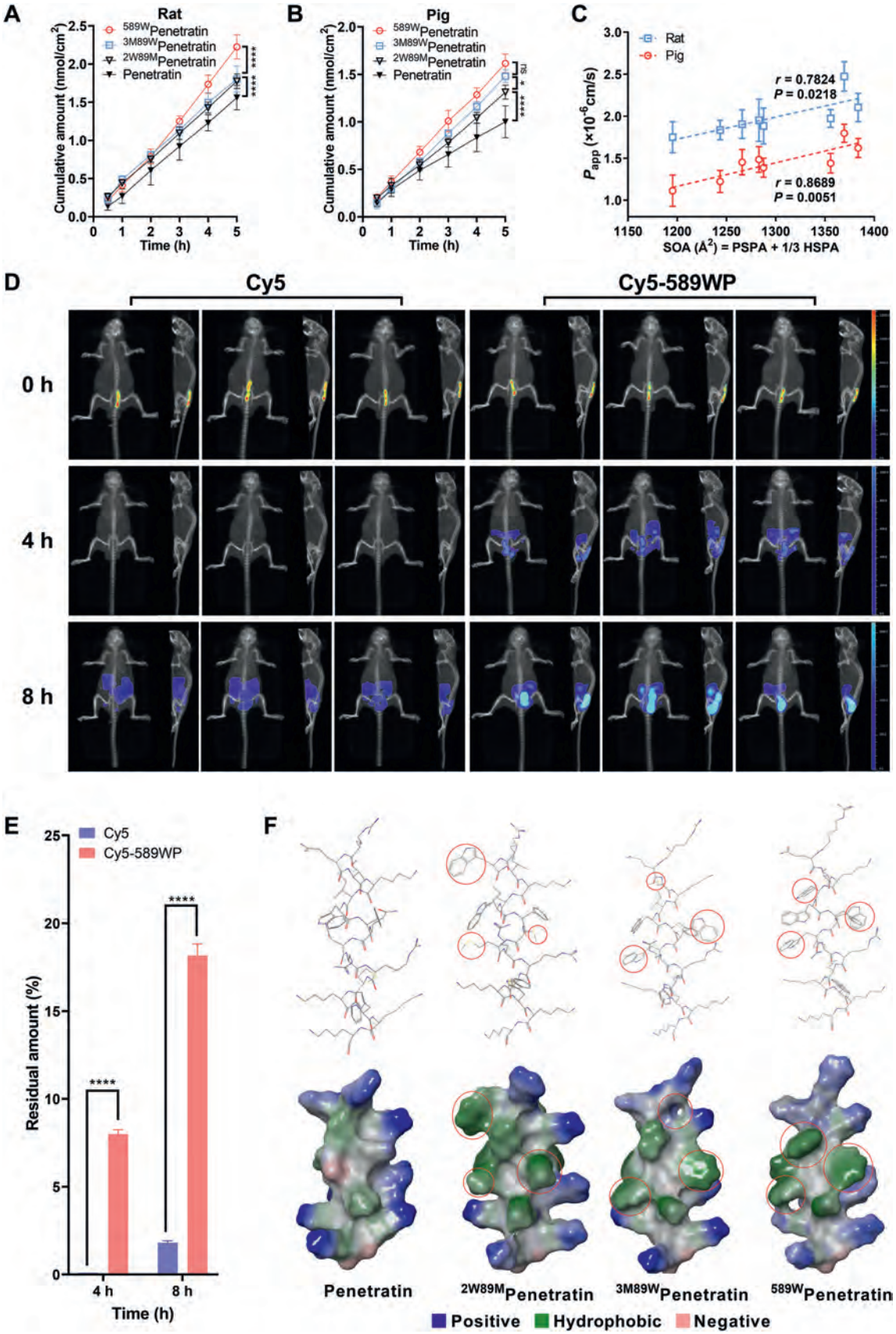

Figure 5 Experimental verification of transdermal penetration enhancement *ex vivo* and *in vivo*. (A, B) Cumulative amount-time curves of the wild-type penetratin and its derivatives in excised skin: (A) rat skin, (B) pig skin ($n = 4$). (C) Correlations between P_{app} values and SOA of the

conformation, that collectively contributed to the increase in PSPA, even in the absence of introducing basic amino acids.

After *in vitro* screening, computational simulation, model refinement, sequence prediction, and experimental verification, we have successfully developed a novel peptide, 589WP, with high skin permeability. This peptide exhibited 41% and 62% increase in P_{app} values in rat and pig skin respectively compared to the wild-type penetratin. In addition, FAM-589WP demonstrated a 72 and 60-fold increase in P_{app} values in rat and pig skin respectively compared to free FAM.

3.5. Synthesis of FUdR-589WP conjugate and in vitro evaluation

Using 4-aminobutyric acid as the linker and through a two-step process involving esterification and click chemistry reactions (Fig. 6A), we successfully synthesized the isomeric FUdR-589WP conjugates. Products were purified by HPLC and characterized by NMR and MS analyses (Supporting Information Figs. S4 and S5). To evaluate whether covalent conjugation could impact the antitumor efficacy of FUdR, we compared the cytotoxicity of free 589WP, free FUdR, intermediate FUdR-Mal, and final product FUdR-589WP in B16F10 cells (Fig. 6B and C). It is specifically noted that the isomers of both FUdR-Mal-1/2 and FUdR-589WP-1/2 exhibited similar inhibitory effects on B16F10 cells and comparable IC_{50} values (Supporting Information Fig. S6). Therefore, they were combined and collectively designated as FUdR-Mal and FUdR-589WP. Free 589WP showed low toxicity to melanoma cells with an IC_{50} higher than 150 μmol/L. In comparison to free FUdR, the IC_{50} of FUdR-Mal and FUdR-589WP significantly increased ($P < 0.0001$ for FUdR-Mal and $P < 0.01$ for FUdR-589WP), indicating that covalent conjugation attenuated the antitumor effect. However, due to the penetration-enhancing effect of 589WP, FUdR-589WP still improved the inhibition effect on B16F10 cells at a relatively low concentration (IC_{50} about 15 μmol/L) compared with FUdR-Mal. This was visualized by Calcein-PI staining of B16F10 cells after being treated with 15 μmol/L various agents for 48 h (Fig. 6D). Calcein can stain live cells green, while PI can stain dead cells red. In the control group and the group treated with free 589WP, similar live cell density and no dead cells were observed, indicating that 589WP alone did not affect tumor cell survival. In contrast, the group treated with free FUdR exhibited a notable decrease in live cell density, while the FUdR-Mal group showed only a slight decrease. Meanwhile, the FUdR-589WP group displayed a nearly 50% live cell density. Dead cells could be observed in all of the FUdR, FUdR-Mal, and FUdR-589WP groups. It's worth noting that the majority of the dead cells could not be observed as they floated in the cell culture medium due to the lack of cell adhesiveness.

FUdR can be barely released at weakly acidic pH, slowly released from FUdR-589WP at physiological pH, and released more rapidly at weakly basic pH (Fig. 6E). It has been demonstrated that the release of FUdR is controlled by cleavage of the ester bond between FUdR and the linker. Moreover, porcine liver esterase (PLE) can accelerate the release of FUdR, which is concentration-dependent (Fig. 6F). Hence, the *in vivo* process of FUdR-589WP can be depicted by cumulative release-time curves. When it penetrates across the epidermis and dermis, the majority of FUdR-589WP remains intact, while only a small amount of FUdR is released at a relatively slow rate under low concentrations of esterase in the weakly acidic skin microenvironment. However, upon reaching the tumor tissue area, where the strong growth demand of melanoma induces a significant increase in esterase concentration[47], FUdR can be rapidly released, thereby exerting its antitumor effects in both FUdR-589WP and free FUdR forms.

3.6. In vivo anti-melanoma efficacy of FUdR-589WP

To assess the *in vivo* therapeutic efficacy of FUdR-589WP gel, we established a subcutaneous melanoma model in mice. The tumor growth curves illustrated that topically applied 0.5% FUdR-589WP gel significantly inhibited subcutaneous melanoma compared to all other groups (Fig. 7A and B, $P < 0.0001$). This result indicates that covalent conjugation with 589WP efficiently improved the skin permeability of FUdR and therefore led to more powerful efficacy even at a reduced concentration (only 1/5 of the 2.5% FUdR gel). In addition, 0.5% FUdR/589WP gel exhibited similar tumor inhibition compared to 2.5% FUdR gel ($P > 0.05$), and both significantly inhibited subcutaneous melanoma compared to the blank gel ($P < 0.0001$), implying physical mixture can also promote transdermal absorption of FUdR. However, physical mixture was significantly less efficient than covalent conjugation ($P < 0.0001$). Neither 0.5% FUdR gel nor 0.05% FUdR-589WP gel exhibited significant inhibition on tumor growth compared to the blank gel ($P > 0.05$), indicating that the antitumor effect of FUdR and FUdR-589WP is concentration-dependent. The differences among all groups were also evident in the dissected melanoma tissues (Fig. 7C). Furthermore, hematoxylin-eosin (HE) stained sections of the main organs and the skin exposed to various formulations are shown in Supporting Information Figs. S7 and S8, and no noticeable toxicity was observed.

As high dosages of 5-FU and FUdR have the risk of causing skin irritation in clinical practice[37], it is also crucial to improve the safety of the marketed products. To evaluate the skin irritation caused by the formulations, healthy mice were used as the animal model. After administering the gels for 7 days, immunohistochemistry (IHC) staining with the IL-1β antibody was performed on the skin at the application site, and the brown color represents immune-positive regions (Fig. 7D). The results revealed that both the 0.5% FUdR and 2.5% FUdR gels induced more immune-positive reactions (indicated by the black arrow) and deeper brown staining compared to the control group. In contrast, 0.5% 589WP or 0.5% FUdR-589WP gels did not show similar effects, suggesting that these formulations are less likely to cause obvious skin irritation. Further support for this conclusion comes from the semi-quantitative average optical density (AOD) values of all groups (Fig. 7E). The AOD values of 0.5% 589WP and FUdR-589WP groups did not exhibit a statistically significant difference compared to that of the control group ($P > 0.05$), and

wild-type penetratin and its derivatives in rat and pig skin ($n = 4$). (D) Fluorescence molecular tomography (FMT) and computed tomography (CT) merged images of mice treated with Cy5 or Cy5-589WP gel ($n = 3$). (E) The semi-quantitative residual amount of Cy5 and Cy5-589WP *in vivo* ($n = 3$). (F) Predicted peptide folding structures and surface patch area distribution (The red circles mark the sites of mutated amino acids. Blue represents the positive surface patch, green represents the hydrophobic surface patch, and pink represents the negative surface patch). Data are presented as mean ± SD. *$P < 0.05$ and ****$P < 0.0001$ *vs*. indicated; ns, not significant.

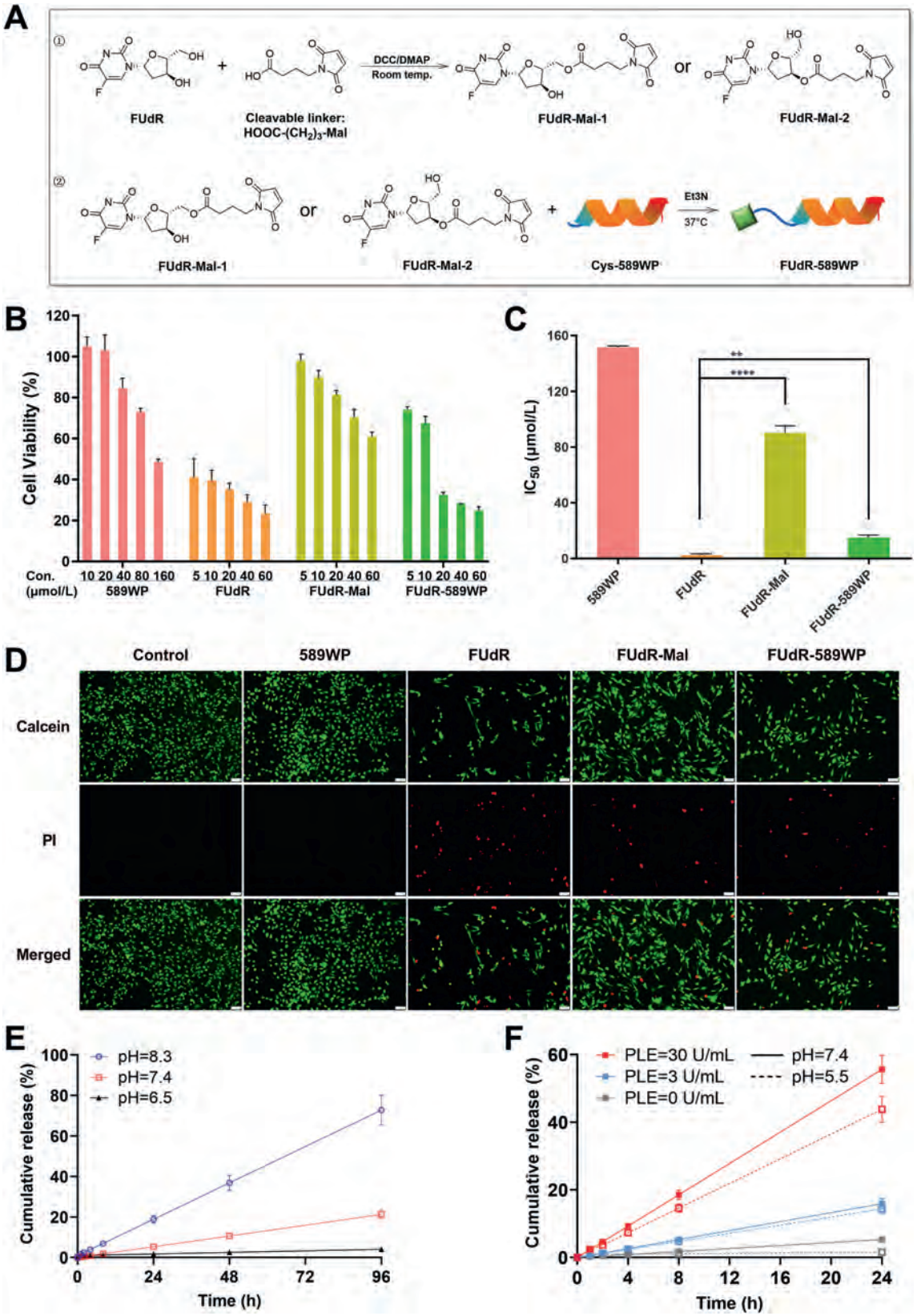

Figure 6 Synthesis route of FUdR-589WP, *in vitro* cytotoxicity, and drug release. (A) Synthesis route of FUdR-589WP: (i) Esterification reaction between FUdR and 4-maleimidobutyric acid catalyzed by DCC/DMAP. (ii) Click chemistry reaction between maleimide of FUdR-Mal and sulfhydryl group of Cys-589WP. (B) B16F10 cell viability after treated with 589WP, FUdR, FUdR-Mal, and FUdR-589WP for 48 h ($n = 5$). (C) IC_{50} values of 589WP, FUdR, FUdR-Mal, and FUdR-589WP in B16F10 cells after co-incubation for 48 h ($n = 5$). (D) Calcein-PI staining images of B16F10 cells after treated with 15 μmol/L 589WP, FUdR, FUdR-Mal, and FUdR-589WP for 48 h. (E) Cumulative release-time curves

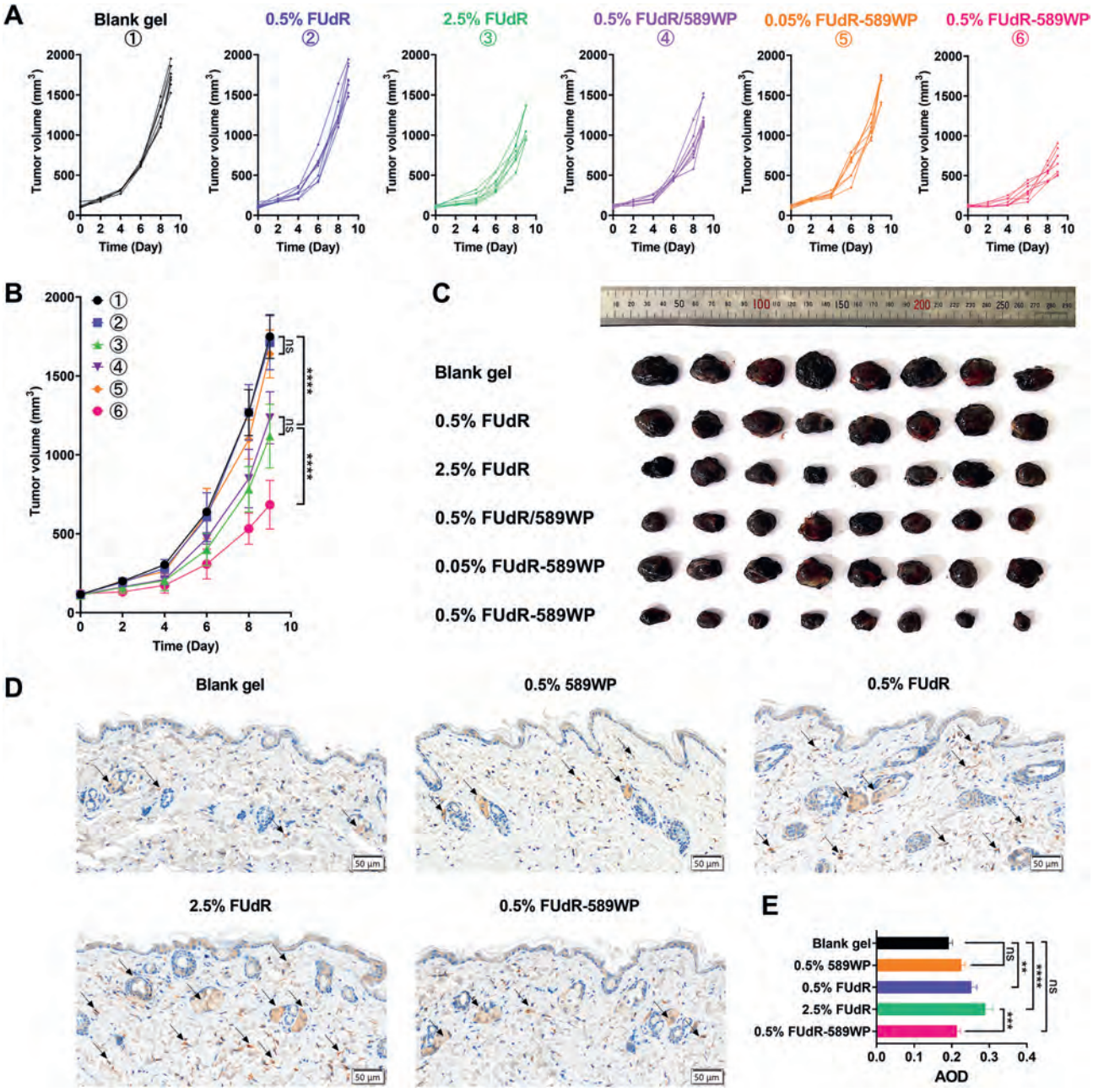

Figure 7 Anti-melanoma efficacy in mice and safety evaluation. (A) Independent tumor volume-time curves of blank gel, 0.5% FUdR, 2.5% FUdR, 0.5% FUdR/589WP, 0.05% FUdR-589WP, and 0.5% FUdR-589WP gels ($n = 8$). (B) Comparison between tumor volume-time curves of all groups ($n = 8$). (C) Dissected melanoma issues of all groups ($n = 8$). (D) Immunohistochemistry (IHC) staining with the IL-1β antibody of skin sections. (E) Semi-quantitative average optical density (AOD) values of IHC sections ($n = 3$). All gels were administered once a day to the skin above the melanoma area in C57BL/6 mice since tumor volume exceeded 100 mm^3, with blank gel used as a negative control. The gel matrix consisted of 50% glycerin, 30% PEG 200, and 20% PEG 400 (*w*/*w*). Black arrows indicate the positive signals (scale bar = 50 μm). Data are presented as mean ± SD. $^{**}P < 0.01$, $^{***}P < 0.001$, and $^{****}P < 0.0001$ *vs.* indicated; ns, not significant.

meanwhile, they were significantly lower than that of the 2.5% FUdR group ($P < 0.01$). This difference could be attributed to the reduced dosage of 0.5% FUdR-589WP gel, which was only 1/5 of the 2.5% FUdR formulation. Since 589WP is inherently safe as a peptide, it contributes to the overall safety profile of the formulation. Additionally, the sustained release of FUdR from the conjugate also facilitates lower irritancy compared to free FUdR at the same dosage. Taken together, the results of antitumor efficacy,

of FUdR at different pH conditions ($n = 3$). (F) Cumulative release-time curves of FUdR with various concentrations of porcine liver esterase (PLE) at pH 7.4 and 5.5 ($n = 3$). Data are presented as mean ± SD. $^{**}P < 0.01$ and $^{****}P < 0.0001$ *vs.* indicated.

HE, and IHC staining collectively indicate that 589WP is an efficient and safe skin permeation enhancer.

4. Discussion

The majority of small molecule drugs and almost all biological macromolecules are difficult to penetrate the skin barrier. Permeation enhancers are crucial for improving the transdermal drug absorption. Classical permeation enhancers are mainly chemicals, such as terpenes, esters, lactams, fatty acids or alcohols, and derivatives of sugars, vitamins, or amino acids. They generally act on the intercellular stratum corneum lipids, the main permeation pathway for most drugs[48]. Continuous application of non-biodegradable chemicals at high concentrations would increase the risk of potential irritation and toxicity. An ideal permeation enhancer should enhance transdermal delivery without irreversibly damaging skin or compromising its normal barrier function[49].

It was previously reported that amino acid-based amphiphiles showed high and reversible activity, along with low dermal irritation and toxicity[4], which suggests a promising direction for permeation enhancers development. CPPs have already been used for transdermal delivery of various types of drugs, although still in the early stages of development. For instance, penetratin[22], and transportan[28] were separately incorporated in the reversed hexagonal mesophases or microemulsions to improve the topical absorption of sodium diclofenac and paclitaxel. In these studies, the CPPs promoted a less than 2-fold increase in the cumulative transport crossing the skin. We demonstrated herein that the skin permeability of fluorescent probe FAM was enhanced more than 51-fold when conjugated with these CPPs. Covalent conjugation with CPP is a more efficient strategy for transdermal drug delivery, which even could enable biological macromolecules to be absorbed topically. The immunosuppressive protein FK506B fused to Pep-1 effectively inhibited allergic dermatitis *via* transdermal delivery[25]. In addition to linear CPPs, cyclic peptides are also used as skin permeation enhancers. SPACE, a cyclic peptide identified by phage display, facilitates the penetration of conjugated cargoes across the stratum corneum into the epidermis and dermis[50]. The skin penetration of cyclosporine was also enhanced by approximately 2.5-fold in the presence of SPACE[12]. As shown in Fig. 1, SPACE demonstrated significantly higher permeability than free FAM; however, it exhibited only about half the permeability of wild-type penetratin and about one-third the permeability of the optimized peptide 589WP.

Molecular level determinants of skin permeation remains incompletely understood. The molecular transport theories attribute permeation enhancement by chemical substances to their physicochemical properties, described by the solubility parameters, including hydrogen bonding, polar interactions, and dispersive interactions[4]. For skin-penetrating peptides, previous studies have shown that skin permeability was related to α-helix and charge interactions[51]. However, this simple rule couldn't explain why those peptides without α-helix or with less positive charges sometimes performed better in transdermal delivery. This inspired us to conduct a deeper exploration of the relationship between the physicochemical properties of peptides and their skin permeability.

Through integrating the results from experimental determination and computer simulation, we found that among numerous physicochemical properties, the skin permeability of CPPs was related to their positive surface patch areas (PSPA), hydrogen bond donor areas (HBDA), and net charge. Upon further analysis, only PSPA emerged as a statistically significant factor, but it was also demonstrated not the sole essential factor affecting the skin permeability. A recent review highlighted that effective transdermal CPPs are rich in charged residues, with low instability and aliphatic indices[52]. We amended and quantified this theory by introducing parameters PSPA and hydrophobic surface patch areas (HSPA), and then proposed the concept of score of amphipathy (SOA = PSPA + 1/3 HSPA). Using this predictive model, we screened more than 1500 peptide sequences, and the accuracy achieved a correlation coefficient higher than 0.85 for the selected penetratin derivatives when validated using excised pig skin. Moreover, the redesigned peptide, based on this predictive model, exhibited enhanced *in vivo* skin permeability and topical anti-melanoma efficacy when covalently conjugated with the chemotherapeutic drug FUdR.

As the name "score of amphipathy" suggests, the SOA aims to link the microscopic peptide surface area with its macroscopic amphipathy, highlighting its physical and chemical significance. In previous studies, positive charge is a well-established determinant of skin permeability. The cationic charge from arginine and lysine residues in CPPs or CPP-drug conjugates enhances their binding to negatively charged cell membrane and extracellular matrix (ECM) components like heparin sulfate, phospholipids, and keratin in the stratum corneum (SC) barrier[6]. This creates an electrical potential gradient, which generates inward-pointing electric fields and provides a driving force that plays a significant role in the translocation and penetration of CPPs into different layers of the skin[53]. As shown in Fig. 3E and F, our research has also revealed that skin permeability is closely related to the parameters PSPA and charge. The relationship between hydrophobicity and skin permeability is well-established and widely recognized in pharmaceutical sciences. As shown in Fig. 3B−D, our research has further demonstrated that skin permeability is closely related to the parameter HSPA in hydrophobic CPPs, but not in cationic or amphipathic ones. It is worth noting that PSPA and HSPA are interdependent variables, meaning that changes in PSPA inevitably lead to changes in HSPA. Therefore, the lack of correlation between skin permeability and HSPA in cationic or amphipathic CPPs might be concealed by the more influential factor, PSPA. Thus, the inclusion of HSPA in optimizing the model was reasonable and also based on an understanding of amphipathy. Specifically, SOA reflects the peptide's positive charge and hydrophobicity, which influence skin permeability and biological activity.

Currently, 5% 5-FU cream has been approved by the FDA for the treatment of various skin conditions, including actinic keratosis (AK)[54], superficial basal cell carcinoma (BCC)[40], and squamous cell carcinoma *in situ* (Bowen's Disease)[55]. Additionally, 5-FU injections have been used for the treatment of other skin disorders, such as keloids and hypertrophic scars[56]. All these conditions could potentially benefit from the topical delivery of 0.5% FUdR-589WP, which can be converted to 5-FU by thymidine phosphorylase. This approach effectively replaces the higher 5% dosage of free 5-FU and significantly reduces potential skin irritation in the treatment of AK, BCC, and Bowen's Disease. Moreover, for keloids and hypertrophic scars, it provides a less painful and more convenient alternative to large-area, multiple injections administered.

5. Conclusions

In conclusion, based on extensive comparison and screening, we elucidated the main physicochemical factors affecting CPPs'

permeability and designed a novel skin-penetrating peptide, 589WP. When one small molecule, for example, FAM, was covalently conjugated with 589WP, its skin permeability could be efficiently increased by up to 72 times. In the topical treatment of melanoma, both the combination and conjugation of FUdR and 589WP significantly inhibited tumor growth at a reduced dosage (only 1/5 of the standard dosage in clinical practice). As the dosage was reduced, in addition to the inherent biodegradability and biocompatibility of the peptide, the overall gel formulation exhibited excellent safety. The remarkable transdermal efficiency of 589WP was accurately predicted by the SOA model. To our knowledge, the SOA model is the first quantitative method to assess the amphipathy of peptides at the molecular level, and it reveals the key properties of peptides correlated with skin permeability. The peptide prediction and design workflow established in this study offers a great potential for guiding the development of skin permeation enhancers. Nevertheless, it remains unknown how the peptide transports cargo through intact skin barriers, necessitating further research to elucidate the relevant processes and mechanisms. Moreover, the applicability of the prediction model based on SOA to other categories of CPPs still requires further experimental validation.

Acknowledgments

This work was supported by the National Natural Science Foundation of China (82273864), the National Key R&D Program of China (2024YFA1210203), the Seed Program for Medical New Technology Research and Translation of the Shanghai Municipal Health Commission (2025ZZ1020, China), and the Shanghai Science and Technology Program (21ZR1407100 and 21S11905300, China). Thanks to Schrödinger company for offering free Maestro to academia.

Author contributions

Sanjiang Du: Methodology, Validation, Formal analysis, Investigation, Data Curation, Writing − original draft preparation, Writing − Review & Editing, Visualization. Hanlin Wang: Methodology, Software, Formal analysis. Feiyang Geng: Investigation, Visualization. Zongxu Zhang: Investigation. Chenghao Liu: Investigation. Weiyue Lu: Conceptualization, Resources, Project administration. Gang Wei: Conceptualization, Methodology, Resources, Writing − review & editing, Supervision, Project administration, Funding acquisition.

Conflicts of interest

The authors declare no conflict of interest.

Appendix A. Supporting information

Supporting information to this article can be found online at https://doi.org/10.1016/j.apsb.2025.12.026.

References

1. Prausnitz MR, Langer R. Transdermal drug delivery. *Nat Biotechnol* 2008;**26**:1261−8.
2. Marwah H, Garg T, Rath G, Goyal AK. Development of transferosomal gel for trans-dermal delivery of insulin using iodine complex. *Drug Deliv* 2016;**23**:1636−44.
3. Pandey PC, Shukla S, Skoog SA, Boehm RD, Narayan RJ. Current advancements in transdermal biosensing and targeted drug delivery. *Sensors* 2019;**19**:1028.
4. Karande P, Jain A, Ergun K, Kispersky V, Mitragotri S. Design principles of chemical penetration enhancers for transdermal drug delivery. *Proc Natl Acad Sci U S A* 2005;**102**:4688−93.
5. Chen Y, Wang M, Fang L. Biomaterials as novel penetration enhancers for transdermal and dermal drug delivery systems. *Drug Deliv* 2013;**20**:199−209.
6. Vedadghavami A, Zhang C, Bajpayee AG. Overcoming negatively charged tissue barriers: drug delivery using cationic peptides and proteins. *Nano Today* 2020;**34**:100898.
7. Bouwstra JA, Nădăban A, Bras W, McCabe C, Bunge A, Gooris GS. The skin barrier: an extraordinary interface with an exceptional lipid organization. *Prog Lipid Res* 2023;**92**:101252.
8. Alexander A, Dwivedi S, Ajazuddin Giri TK, Saraf S, Tripathi DK. Approaches for breaking the barriers of drug permeation through transdermal drug delivery. *J Control Release* 2012;**164**:26−40.
9. Wong TW. Electrical, magnetic, photomechanical and cavitational waves to overcome skin barrier for transdermal drug delivery. *J Control Release* 2014;**193**:257−69.
10. Subedi RK, Oh SY, Chun MK, Choi HK. Recent advances in transdermal drug delivery. *Arch Pharm Res (Seoul)* 2010;**33**:339−51.
11. Lian Z, Ji T. Functional peptide-based drug delivery systems. *J Mater Chem B* 2020;**8**:6517−29.
12. Kumar S, Zakrewsky M, Chen M, Menegatti S, Muraski JA, Mitragotri S. Peptides as skin penetration enhancers: mechanisms of action. *J Control Release* 2015;**199**:168−78.
13. Yang R, Wei T, Goldberg H, Wang W, Cullion K, Kohane DS. Getting drugs across biological barriers. *Adv Mater* 2017;**29**:1606596.
14. Zhou M, Zou X, Cheng K, Zhong S, Su Y, Wu T, et al. The role of cell-penetrating peptides in potential anti-cancer therapy. *Clin Transl Med* 2022;**12**:e822.
15. Nasrollahi SA, Taghibiglou C, Azizi E, Farboud ES. Cell-penetrating peptides as a novel transdermal drug delivery system. *Chem Biol Drug Des* 2012;**80**:639−46.
16. Kim YC, Ludovice PJ, Prausnitz MR. Transdermal delivery enhanced by magainin pore-forming peptide. *J Control Release* 2007;**122**:375−83.
17. Lin L, Chi J, Yan Y, Luo R, Feng X, Zheng Y, et al. Membrane-disruptive peptides/peptidomimetics-based therapeutics: promising systems to combat bacteria and cancer in the drug-resistant era. *Acta Pharm Sin B* 2021;**11**:2609−44.
18. Chen Y, Shen Y, Guo X, Zhang C, Yang W, Ma M, et al. Transdermal protein delivery by a coadministered peptide identified *via* phage display. *Nat Biotechnol* 2006;**24**:455−60.
19. Kumar S, Sahdev P, Perumal O, Tummala H. Identification of a novel skin penetration enhancement peptide by phage display peptide library screening. *Mol Pharm* 2012;**9**:1320−30.
20. Menegatti S, Zakrewsky M, Kumar S, De Oliveira JS, Muraski JA, Mitragotri S. *De novo* design of skin-penetrating peptides for enhanced transdermal delivery of peptide drugs. *Adv Healthcare Mater* 2016;**5**:602−9.
21. Wang K, Zhao X, Yang F, Liu P, Xing J. Percutaneous delivery application of acylated steric acid-9-p(arginine) cell penetrating peptides used as transdermal penetration enhancer^{+}. *J Biomed Nanotechnol* 2019;**15**:417−30.
22. Cohen-Avrahami M, Libster D, Aserin A, Garti N. Penetratin-induced transdermal delivery from H(II) mesophases of sodium diclofenac. *J Control Release* 2012;**159**:419−28.
23. Gennari CG, Franzè S, Pellegrino S, Corsini E, Vistoli G, Montanari L, et al. Skin penetrating peptide as a tool to enhance the permeation of heparin through human epidermis. *Biomacromolecules* 2016;**17**:46−55.

24. Candan G, Michiue H, Ishikawa S, Fujimura A, Hayashi K, Uneda A, et al. Combining poly-arginine with the hydrophobic counter-anion 4-(1-pyrenyl)-butyric acid for protein transduction in transdermal delivery. *Biomaterials* 2012;**33**:6468−75.
25. Kim SY, Sohn EJ, Kim DW, Jeong HJ, Kim MJ, Kang HW, et al. Transduced PEP-1-FK506BP ameliorates atopic dermatitis in NC/Nga mice. *J Invest Dermatol* 2011;**131**:1477−85.
26. Manosroi J, Lohcharoenkal W, Götz F, Werner RG, Manosroi W, Manosroi A. Transdermal absorption and stability enhancement of salmon calcitonin by Tat peptide. *Drug Dev Ind Pharm* 2013;**39**: 520−5.
27. Kim YC, Late S, Banga AK, Ludovice PJ, Prausnitz MR. Biochemical enhancement of transdermal delivery with magainin peptide: modification of electrostatic interactions by changing pH. *Int J Pharm* 2008;**362**:20−8.
28. Pepe D, Carvalho VF, McCall M, de Lemos DP, Lopes LB. Transportan in nanocarriers improves skin localization and antitumor activity of paclitaxel. *Int J Nanomed* 2016;**11**:2009−19.
29. Vij M, Natarajan P, Pattnaik BR, Alam S, Gupta N, Santhiya D, et al. Non-invasive topical delivery of plasmid DNA to the skin using a peptide carrier. *J Control Release* 2016;**222**:159−68.
30. Rothbard JB, Garlington S, Lin Q, Kirschberg T, Kreider E, McGrane PL, et al. Conjugation of arginine oligomers to cyclosporin A facilitates topical delivery and inhibition of inflammation. *Nat Med* 2000;**6**:1253−7.
31. Lopes LB, Brophy CM, Furnish E, Flynn CR, Sparks O, Komalavilas P, et al. Comparative study of the skin penetration of protein transduction domains and a conjugated peptide. *Pharm Res* 2005;**22**:750−7.
32. Carmichael NME, Dostrovsky JO, Charlton MP. Peptide-mediated transdermal delivery of botulinum neurotoxin type A reduces neurogenic inflammation in the skin. *Pain* 2010;**149**:316−24.
33. Hou YW, Chan MH, Hsu HR, Liu BR, Chen CP, Chen HH, et al. Transdermal delivery of proteins mediated by non-covalently associated arginine-rich intracellular delivery peptides. *Exp Dermatol* 2007;**16**:999−1006.
34. Jumper J, Evans R, Pritzel A, Green T, Figurnov M, Ronneberger O, et al. Highly accurate protein structure prediction with AlphaFold. *Nature* 2021;**596**:583−9.
35. Baek M, DiMaio F, Anishchenko I, Dauparas J, Ovchinnikov S, Lee GR, et al. Accurate prediction of protein structures and interactions using a three-track neural network. *Science* 2021;**373**:871−6.
36. Domingues B, Lopes JM, Soares P, Pópulo H. Melanoma treatment in review. *ImmunoTargets Ther* 2018;**7**:35−49.
37. Peng LH, Wang MZ, Chu Y, Zhang L, Niu J, Shao HT, et al. Engineering bacterial outer membrane vesicles as transdermal nanoplatforms for photo-TRAIL-programmed therapy against melanoma. *Sci Adv* 2020;**6**:2735.
38. Pinedo HM, Peters GF. Fluorouracil: biochemistry and pharmacology. *J Clin Oncol* 1988;**6**:1653−64.
39. Longley DB, Harkin DP, Johnston PG. 5-fluorouracil: mechanisms of action and clinical strategies. *Nat Rev Cancer* 2003;**3**:330−8.
40. Kim JYS, Kozlow JH, Mittal B, Moyer J, Olencki T, Rodgers P. Guidelines of care for the management of basal cell carcinoma. *J Am Acad Dermatol* 2018;**78**:540−59.
41. Weinstock MA, Thwin SS, Siegel JA, Marcolivio K, Means AD, Leader NF, et al. Chemoprevention of basal and squamous cell carcinoma with a single course of fluorouracil, 5%, cream: a randomized clinical trial. *JAMA Dermatol* 2018;**154**:167−74.
42. Hasan N, Nadaf A, Imran M, Jiba U, Sheikh A, Almalki WH, et al. Skin cancer: understanding the journey of transformation from conventional to advanced treatment approaches. *Mol Cancer* 2023;**22**: 168.
43. Cunningham TJ, Tabacchi M, Eliane JP, Tuchayi SM, Manivasagam S, Mirzaalian H, et al. Randomized trial of calcipotriol combined with 5-fluorouracil for skin cancer precursor immunotherapy. *J Clin Investig* 2017;**127**:106−16.
44. Mirdita M, Schütze K, Moriwaki Y, Heo L, Ovchinnikov S, Steinegger M. ColabFold: making protein folding accessible to all. *Nat Methods* 2022;**19**:679−82.
45. Hoang HN, Hill TA, Fairlie DP. Connecting hydrophobic surfaces in cyclic peptides increases membrane permeability. *Angew Chem Int Ed Engl* 2021;**60**:8385−90.
46. Pescina S, Ostacolo C, Gomez-Monterrey IM, Sala M, Bertamino A, Sonvico F, et al. Cell penetrating peptides in ocular drug delivery: state of the art. *J Control Release* 2018;**284**:84−102.
47. Zhao D, Zhang H, Tao W, Wei W, Sun J, He Z. A rapid albumin-binding 5-fluorouracil prodrug with a prolonged circulation time and enhanced antitumor activity. *Biomater Sci* 2017;**5**: 502−10.
48. Kováčik A, Kopečná M, Vávrová K. Permeation enhancers in transdermal drug delivery: benefits and limitations. *Expet Opin Drug Deliv* 2020;**17**:145−55.
49. Ahad A, Aqil M, Kohli K, Chaudhary H, Sultana Y, Mujeeb M, et al. Chemical penetration enhancers: a patent review. *Expert Opin Ther Pat* 2009;**19**:969−88.
50. Hsu T, Mitragotri S. Delivery of siRNA and other macromolecules into skin and cells using a peptide enhancer. *Proc Natl Acad Sci U S A* 2011;**108**:15816−21.
51. Chang M, Li X, Sun Y, Cheng F, Wang Q, Xie X, et al. Effect of cationic cyclopeptides on transdermal and transmembrane delivery of insulin. *Mol Pharm* 2013;**10**:951−7.
52. Shin HJ, Lee BK, Kang HA. Transdermal properties of cell-penetrating peptides: applications and skin penetration mechanisms. *ACS Appl Bio Mater* 2024;**7**:1−16.
53. Zorko M, Langel U. Cell-penetrating peptides: mechanism and kinetics of cargo delivery. *Adv Drug Deliv Rev* 2005;**57**:529−45.
54. Malvehy J, Stratigos AJ, Bagot M, Stockfleth E, Ezzedine K, Delarue A. Actinic keratosis: current challenges and unanswered questions. *J Eur Acad Dermatol Venereol* 2024;**38**:3−11.
55. Mohandas P, Lowden M, Varma S. Bowen's disease. *BMJ* 2020;**368**: m813.
56. Murakami T, Shigeki S. Pharmacotherapy for keloids and hypertrophic scars. *Int J Mol Sci* 2024;**25**:4674.